SIAM J. SCI. COMPUT.
Vol. 36, No. 5, pp. A2149–A2165

FINITE ELEMENT FORMULATION IN FLAT COORDINATE SPACES TO SOLVE ELLIPTIC PROBLEMS ON GENERAL CLOSED RIEMANNIAN MANIFOLDS*

LIZHEN QIN†, SHANGYOU ZHANG‡, AND ZHIMIN ZHANG§

Abstract. We apply finite element methods to elliptic problems on closed Riemannian manifolds. The elliptic equations on manifolds are reduced to coupled equations on Euclidean spaces by using coordinate charts. The advantage of this strategy is to avoid global triangulations on curved manifolds in the finite element method. The resulting finite element problems can be solved by direct methods or by domain decomposition iterations. We present a convergence theory and some computational results. Our methods are illustrated by a 3-dimensional sphere problem in 4-dimensional Euclidean space. We also give a numerical comparison between the surface finite element method and our methods.

Key words. Riemannian manifolds, elliptic problems, domain decomposition methods, finite element methods

AMS subject classifications. Primary, 65N30; Secondary, 46E25, 20C20

DOI. 10.1137/110854722

1. Introduction.

Elliptic problems on Riemannian manifolds are important both in analysis and in geometry (see [31, 21]). So-called geometric partial differential equations appear in many areas, such as multifluid dynamics, micromagnetics, and image processing; cf. [2, 3, 13, 14, 15, 29, 34, 30]. A simple example is the equation

$$-\Delta_S u + bu = f. \tag{1.1}$$

Here Δ_S is the Laplace–Beltrami operator defined on an n-dimensional manifold M. When solving such an elliptic equation by the finite element method, a challenge is the construction of a grid on the manifold (e.g., a surface grid); cf. [7, 8, 13, 25, 26, 33].

We propose an approach different from constructing such grids on manifolds. For our approach, coordinate charts are introduced in the weak form of (1.1). For example, we have

$$\int_M \langle \nabla_S u, \nabla_S v \rangle = \sum_k \int_{\Omega_k} g_k^{\alpha\beta} \frac{\partial u}{\partial x_\alpha} \frac{\partial v}{\partial x_\beta} \sqrt{G} dx_1 \cdots dx_n \quad \forall v \in H^1(\Omega_k). \tag{1.2}$$

The left-hand side of (1.2) is an integral with respect to the volume form of M, and $\langle \cdot, \cdot \rangle$ is the inner product. (For brevity, we shall omit the volume form in integrals on M throughout this paper.) On the right-hand side of (1.2), $\left(g_k^{\alpha\beta}\right)$ is the inverse matrix of the metric matrix in a coordinate chart $\varphi_k : \Omega_k \to M_k$, and G is the determinant of the metric matrix, where the interiors of M_k are disjoint and $\cup_k M_k = M$. The finite element method is applied inside each Euclidean domain $\Omega_k \subset R^n$. The novelty

*Submitted to the journal's Methods and Algorithms for Scientific Computing section November 10, 2011; accepted for publication (in revised form) June 10, 2014; published electronically September 11, 2014.
http://www.siam.org/journals/sisc/36-5/85472.html
†Department of Mathematics, Purdue University, West Lafayette, IN 47907 (qinl@math.purdue.edu).
‡Department of Mathematical Sciences, University of Delaware, Newark, DE 18716 (szhang@udel.edu).
§Department of Mathematics, Wayne State University, Detroit, MI 48202 (ag7761@wayne.edu).

of this approach is to avoid triangulation on curved manifolds by solving problems on Euclidean spaces.

After choosing coordinate charts of the manifolds, we can easily adopt high-order finite elements and/or uniform grids to achieve high-order accuracy and superconvergence, compared with those on surface grids [7, 8, 13, 33].

When the chosen coordinate charts on M are nonoverlapping and C^1 continuous across the boundary, an elliptic equation can be separated into equations on nonoverlapping subdomains. In this case, the finite element equations can be solved by a direct method, such as the conjugate gradient method. Alternatively, the finite element equations can also be solved by a nonoverlapping domain decomposition iteration. For example, the optimized Schwarz nonoverlapping method [5, 24, 27, 9, 10, 16, 17, 27, 28, 32] can be easily implemented. The same idea appeared in [12], which computed a global conformal map by a nonoverlapping domain decomposition method.

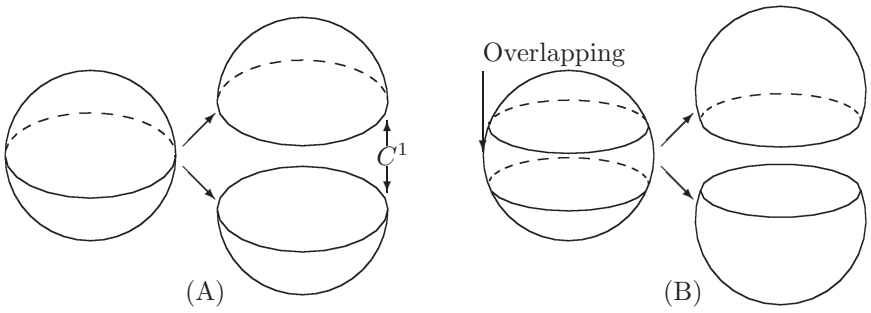

FIG. 1. *Nonoverlapping (left) and overlapping (right) local charts.*

As nonoverlapping charts may not be easily constructed in general (cf. Figure 1), we shall also consider overlapping charts. This leads to an overdetermined but consistent variational problem on the continuous level. (Actually, there is one differential equation associated with each subdomain. Suppose a specific point y belongs to different subdomains. Then the solution value $u(y)$ at y will appear in more than one equation, which means the problem is overdetermined. However, since the solution $u(y)$ exists, the problem is also consistent.) On the discrete level, if the finite element grids in different subdomains are identical on the overlapping region, then the discrete problem will be consistent. However, we do not impose such a stringent condition on the overlapping region. Actually, we require only that the nodes in one subdomain Ω_k are compatible with those on the boundaries of other subdomains $\Omega_{k'}$. In this situation, we can still guarantee that the discrete problem is consistent. Therefore, the discrete problem can be solved by a direct method or by an overlapping domain decomposition iteration.

We choose a problem on a 3-dimensional manifold for the numerical test. The method is to be generalized to solving the Einstein's equations, where the space derivatives are computed on a manifold in a 4-dimensional time-space; cf. [1, 22, 36]. It could be very difficult to construct tetrahedral grids on 3-dimensional manifolds. To the best of our knowledge, such a tetrahedral grid has not been done anywhere for the finite element method. In both our nonoverlapping and overlapping methods, we avoid triangulating both an n-manifold M and the boundaries of its submanifolds M_k. In addition, we also compare our method with the traditional finite element method on surface grids by testing a problem on a 2-dimensional sphere.

The outline of this paper is as follows. Section 2 presents a model problem and its variational form. Section 3 defines the finite element method and shows the convergence of the finite element method. Some numerical results are presented in section 4.

2. A model problem and its two variational problem. For fixing the idea, we consider the following elliptic model problem on an n-dimensional compact orientable smooth Riemannian manifold M with $\partial M = \emptyset$.

$$-\Delta_S u + bu = f, \tag{2.1}$$

where Δ_S is the Laplace–Beltrami operator, and $b > 0$ is a constant. We need to address two issues about (2.1). First, in contrast to a usual elliptic problem on a domain of R^n, (2.1) has no boundary condition. If $\partial M \neq \emptyset$, it is necessary to impose some boundary conditions. Second, in contrast to the usual Laplace operator in R^n, $\sum_{\alpha=1}^{n} \frac{\partial^2}{\partial x_\alpha^2}$, the Laplace operator Δ_S on M *cannot* be expressed by *coordinates globally* because M does not have a global coordinate in general. Locally, we can choose a coordinate chart $(x_1, \ldots, x_n)$ for M. In this particular coordinate chart, the Riemannian metric tensor is expressed as

$$g = \sum_{\alpha,\beta=1}^{n} g_{\alpha\beta} dx_\alpha \otimes dx_\beta,$$

where the matrix $(g_{\alpha\beta})_{n\times n}$ is symmetric and positive definite. The Laplace operator is as follows:

$$\Delta_S u = \frac{1}{\sqrt{G}} \sum_{\alpha=1}^{n} \frac{\partial}{\partial x_\alpha} \left(\sum_{\beta=1}^{n} g^{\alpha\beta} \sqrt{G} \frac{\partial u}{\partial x_\beta} \right),$$

where $G = \det\left((g_{\alpha\beta})_{n\times n}\right)$ is the determinant of the matrix $(g_{\alpha\beta})_{n\times n}$ and $(g^{\alpha\beta})_{n\times n}$ is the inverse of $(g_{\alpha\beta})_{n\times n}$.

In order to translate (2.1) into an equivalent variational problem, we need the volume form and Green formula on an oriented Riemannian manifold with boundary. Locally, the volume form is $\sqrt{G} dx_1 \wedge \cdots \wedge dx_n$, and

$$\nabla_S u = \sum_{\alpha,\beta=1}^{n} g^{\alpha\beta} \frac{\partial u}{\partial x_\alpha} \frac{\partial}{\partial x_\beta}$$

is the gradient of u. If v is another function, we can compute the inner product,

$$\langle \nabla_S u, \nabla_S v \rangle = \sum_{\alpha,\beta=1}^{n} g^{\alpha\beta} \frac{\partial u}{\partial x_\alpha} \frac{\partial v}{\partial x_\beta}.$$

Then we can consider the Riemannian integral $\int_M \Delta_S u$ and $\int_M \langle \nabla_S u, \nabla_S v \rangle$ on M. In general, if f is a function, we can consider its Riemannian integral on M. Locally, in some open subset Ω_k, it is an integral

$$\int_{\Omega_k} f(x_1, \ldots, x_n) \sqrt{G} dx_1 \wedge \cdots \wedge dx_n = \int_{\Omega_k} f(x_1, \ldots, x_n) \sqrt{G} dx_1 \cdots dx_n,$$

where the right-hand side of the above equality is a multiple integral over a domain in R^n. Now we have the following Green formula.

THEOREM 2.1 (Green formula). *If M is a compact orientable Riemannian manifold, $u, v \in C^\infty(M)$, then we have*

$$\int_M \langle -\Delta_S u, v\rangle = \int_M \langle \nabla_S u, \nabla_S v\rangle - \int_{\partial M} \frac{\partial_S u}{\partial \mathbf{n}} v, \tag{2.2}$$

where $\mathbf{n}$ is the outward normal vector on ∂M, and $\frac{\partial_S u}{\partial \mathbf{n}} = \langle \nabla u, \mathbf{n}\rangle$ the outward normal derivative.

Just like the situation of R^n, we can also define distributions on M which are called *currents* (see [11, 20]). Hence Theorem 2.1 can be extended to the case of functions with weak derivatives. We can change (2.1) to a variational form. Since we assume $\partial M = \emptyset$ for (2.1), we have $\int_{\partial M} \frac{\partial_S u}{\partial \mathbf{n}} = 0$. Thus we get

$$\int_M \langle \nabla_S u, \nabla_S v\rangle + \int_M buv = \int_M fv \qquad \forall v \in C^\infty(M). \tag{2.3}$$

After choosing coordinate charts for M, we would get a variational form with boundary integrals. Depending on whether such charts are overlapping or not, we have two different variational forms.

Let $\{\varphi_i\}$ be a C^1 nonoverlapping set of coordinate charts on M. That is, there is a finite set of mappings φ_i such that

$$\begin{aligned} &\varphi_i \ : \ \Omega_i \to M_i, \quad \varphi_i \in C^1(\Omega_i), \quad \Omega_i \subset R^n, \\ &M_i \cap M_j = \emptyset, \quad i \neq j, \quad M = \text{interior}(\cup_i \overline{M}_i), \\ &\frac{\partial \varphi_i^{-1}}{\partial \mathbf{n}_i} = -\frac{\partial \varphi_j^{-1}}{\partial \mathbf{n}_j} \quad \text{on interface } \gamma_{ij} = \partial M_i \cap \partial M_j, \end{aligned} \tag{2.4}$$

where $\mathbf{n}_i$ is the unit out normal to M_i, and γ_{ij} is an $(n-1)$-dimensional, smooth manifold.

We note that we require φ_i be continuously differentiable across the boundary so that the boundary integral in the variational form vanishes. But this can be done only for few special manifolds such as n-sphere or n-torus or their smooth perturbations. In general, the coordinate charts might not be made C^1 across nonoverlapping subdomain boundary on M. In this case we would use overlapping charts to cover M, which leads to an overlapping domain decomposition.

Next is the equivalence theorem under nonoverlapping C^1 charts.

THEOREM 2.2. *Let $\{\varphi_i\}$ be a C^1 nonoverlapping set of coordinate charts on M, defined in* (2.4). *The solution $u((\varphi_i)^{-1}(\mathbf{y}))$ of* (2.1) *is the unique solution of the following variational problem: find*

$$u(\mathbf{x}) \in \{\oplus H^1(\Omega_i) \mid \ u((\varphi_i^{-1}(\mathbf{x})) \text{ can be glued together as a function in } H^1(M)\}$$

such that

$$\sum_i \int_{\Omega_i} \left(\sum_{\alpha,\beta=1}^n g_i^{\alpha\beta} \frac{\partial u}{\partial x_\alpha} \frac{\partial v}{\partial x_\beta} + buv - fv \right) \sqrt{G^{(i)}} d\mathbf{x} = 0 \tag{2.5}$$

for all $v(\mathbf{x}) \in (\oplus H^1(\Omega_i))$. Here $H^1(\Omega_i)$ is the Sobolev space on a Euclidean domain Ω_i.

Proof. Applying the Green formula, Theorem 2.1, on the boundary of each subdomain, we have $u(\varphi_i^{-1}(\mathbf{y}))$ glued together as a global $H^1(M)$ function, and we have a cancellation of boundary integrals, as

$$\int_{\gamma_{ij,x}} \sum_{\alpha,\beta=1}^{n} g_i^{\alpha\beta} \frac{\partial u}{\partial x_\alpha} n_{i,\beta} v d\gamma_x = - \int_{\gamma_{ji,x}} \sum_{\alpha,\beta=1}^{n} g_j^{\alpha\beta} \frac{\partial u}{\partial x_\alpha} n_{j,\beta} v d\gamma_x,$$

where $\gamma_{ij,x} = \{\mathbf{x} \in \overline{\Omega}_i \mid \varphi_i(\mathbf{x}) \in \gamma_{ij}\}$ and $n_{i,\beta}$ (resp., $n_{j,\beta}$) is the βth component of the unit out normal vector on $\gamma_{ij,x}$ (resp., $\gamma_{ji,x}$) with respect to Ω_i (resp., Ω_j). Again, we note that this posts a strong requirement on the coordinate charts $\{\varphi_i\}$; i.e., φ_i^{-1} and φ_j^{-1} are C^1 across γ_{ij}, and γ_{ij} is a smooth (C^1) manifold of $(n-1)$ dimension. ∎

As nonoverlapping C^1 coordinate charts (2.4) may not be possible in general, we introduce next overlapping coordinate charts. The purpose is to avoid all integrals and grids on curved boundaries. Let $\{\varphi_i\}$ be an overlapping set of coordinate charts on M:

$$\begin{aligned} &\varphi_i \ : \ \Omega_i \to M_i, \quad \varphi_i \in C^1(\Omega_i), \quad \Omega_i \subset R^n, \\ &M = \text{interior}(\cup_i \text{interior} M_i). \end{aligned} \tag{2.6}$$

THEOREM 2.3. *Let $\{\varphi_i\}$ be an overlapping set of coordinate charts on M, defined in* (2.6). *The solution $u(\varphi_i^{-1}(\mathbf{y}))$ of* (2.1) *is the unique solution of the following variational problem: find $u(\mathbf{x}) \in \oplus H^1(\Omega_i)$ such that*

$$\begin{aligned} &\int_{\Omega_i} \left(\sum_{\alpha,\beta=1}^{n} g_i^{\alpha\beta} \frac{\partial u}{\partial x_\alpha} \frac{\partial v}{\partial x_\beta} + buv - fv \right) \sqrt{G^{(i)}} d\mathbf{x} = 0 \quad \forall v(\mathbf{x}) \in H_0^1(\Omega_i), \\ &\qquad \textit{and} \ \ u|_{\Omega_i}(\mathbf{x}_i) = u|_{\Omega_j}(\mathbf{x}_j) \quad \textit{if } \varphi_i(\mathbf{x}_i) = \varphi_j(\mathbf{x}_j). \end{aligned} \tag{2.7}$$

Here $H_0^1(\Omega_i)$ is the Sobolev space on a Euclidean domain Ω_i with 0 trace.

Proof. Applying the Green formula, Theorem 2.1, on each submanifold M_i, as $v(\varphi_i^{-1}(\mathbf{y})) \in H_0^1(M_i)$, the solution u of (2.1) satisfies (2.7).

Now we prove the uniqueness of the solution of (2.7). If (2.7) has two solutions u_1 and u_2, then $w = u_1 - u_2$ satisfies the homogeneous equation

$$\int_{\Omega_i} \left(\sum_{\alpha,\beta=1}^{n} g_i^{\alpha\beta} \frac{\partial w}{\partial x_\alpha} \frac{\partial v}{\partial x_\beta} + bwv \right) \sqrt{G^{(i)}} d\mathbf{x} = 0 \quad \forall v \in H_0^1(\Omega_i).$$

In particular, its maximum $w(\mathbf{y}_0) = \max w(M)$ is achieved at some point $\mathbf{y}_0$ within a submanifold M_i. Note that every point of M is inside some M_i. Thus, by the Hopf theorem [19], a generalized maximum principle of Gauss (cf. [18]), we infer $w \equiv w(\mathbf{y}_0)$ on M_i and consequently $w \equiv w(\mathbf{y}_0)$ on whole M. The one-subdomain variational problem leads to $bw = 0$. Thus $w \equiv 0$, which implies $u_1 = u_2$. ∎

3. The finite element method in Euclidean space. We use Euclidean coordinates in the finite element method to solve (2.1). Let M be an n-dimensional oriented Riemannian manifold. We partition M into overlapping or nonoverlapping submanifolds, M_i $(i = 1, \ldots, K)$. Let coordinate charts $\{\varphi_i : \Omega_i \to M_i\}$ be defined either in (2.4) or (2.6). Let $\mathcal{T}_{(i),h}$ be an n-dimensional triangulation on Ω_i:

$$\begin{aligned} \mathcal{T}_{(i),h} = \{T \mid \ &T \text{ is an } n\text{-dimensional, nondegenerate simplex,} \\ &\cup T \approx \Omega_i, \ \text{diam} T \le h\}. \end{aligned}$$

Here a triangulation means that the intersection of any two simplices T_1 and T_2 is a lower dimensional face simplex of both simplices, or an empty set; cf. [6]. For the nonoverlapping charts (2.4), the boundary of Ω_i is usually curved. In this case, if we use P_1 elements in (3.2), $\partial(\cup T)$ approximates $\partial\Omega_i$ to $O(h^2)$, which ensures the optimal approximation of the finite element solution. But if we use higher order finite elements in (3.2), T would be an n-dimensional simplex with one curved face. This is the standard isoparametric finite element [4, 6]; i.e., the finite element reference mapping (not an affine mapping) is a degree k polynomial, the same polynomial order as the finite element space itself. In both cases of nonoverlapping and overlapping coordinate charts, we require a triangulation matching on the interface and the overlapping region (for overlapping charts):

$$\mathcal{T}_h = \{\cup\mathcal{T}_{(i),h} \mid \varphi_i(T_{i,f}) = \varphi_j(T_{j,f_2}) \text{ for some } T_j \in \mathcal{T}_{(j),h} \text{ if } \varphi_i(T_{i,f}) \subset M_j\}, \tag{3.1}$$

where $T_{i,f}$ is either the n-dimensional simplex T_i or one of its $(n-1)$-dimensional face simplices.

Let $V_h^{(i)}$ be the finite element space of order k:

$$V_h^{(i)} = \{v \in H^1(\Omega_i) \mid v|_T \in P_k(x_1, \ldots, x_n) \quad \forall T \in \mathcal{T}_h\}. \tag{3.2}$$

Then we glue these finite element functions together:

$$V_h = \{v \in V_h^{(i)} \mid v(\varphi_i^{-1}(\mathbf{y})) = v(\varphi_j^{-1}(\mathbf{y})) \quad \forall \mathbf{y} \in \overline{M}_i \cap \overline{M}_j\}. \tag{3.3}$$

To be precise, a function of V_h is defined on multiple domains. For example, a nodal basis function $b_k(\mathbf{x})$, associated with a node $\mathbf{y}_k \in \overline{M}_i \cap \overline{M}_j$, is defined by

$$b_k(\mathbf{x}) = \begin{cases} b_k^{(i)}(\mathbf{x}), & \mathbf{x} \in \Omega_i, \\ b_k^{(i)}(\mathbf{x}), & \mathbf{x} \in \Omega_j, \end{cases}$$

$$b_k^{(i)}(\mathbf{x}) = \begin{cases} 1 & \mathbf{x} = \mathbf{x}_k^{(i)}, \\ 0 & \text{rest nodes of } \mathcal{T}_{(i),h}, \end{cases} \qquad b_k^{(i)}(\mathbf{x}) \in V_h^{(i)},$$

$$b_k^{(j)}(\mathbf{x}) = \begin{cases} 1 & \mathbf{x} = \mathbf{x}_k^{(j)}, \\ 0 & \text{rest nodes of } \mathcal{T}_{(j),h}, \end{cases} \qquad b_k^{(i)}(\mathbf{x}) \in V_h^{(j)}.$$

(See Figure 2.) In other words, b_k is defined piecewise on Ω_i and Ω_j, and it is defined globally on M via two inverse mappings.

The finite element method, discretizing the nonoverlapping variational problem (2.5), is simply solving $u_h \in V_h$ such that

$$a(u_h, v_h) = (f, v_h) \quad \forall v_h \in V_h, \tag{3.4}$$

where the bilinear forms are defined by

$$a(u_h, v_h) = \sum_i a_i(u_h, v_h) \quad \text{with}$$

$$a_i(u_h, v_h) = \int_{\Omega_i} \left(\sum_{\alpha,\beta=1}^{n} g_i^{\alpha\beta} \frac{\partial u_h}{\partial x_\alpha} \frac{\partial v_h}{\partial x_\beta} + b u_h v_h \right) \sqrt{G^{(i)}} d\mathbf{x},$$

$$(f, v_h) = \sum_i \int_{\Omega_i} f v_h \sqrt{G^{(i)}} d\mathbf{x}.$$

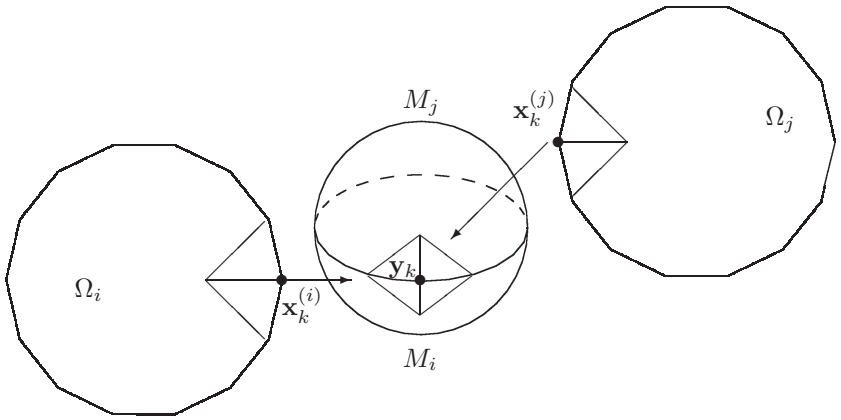

FIG. 2. *Both* $\mathbf{x}_k^{(i)}$ *and* $\mathbf{x}_k^{(j)}$ *are mapped to* $\mathbf{y}_k$, $\mathbf{y}_k = \varphi_i(\mathbf{x}_k^{(i)}) = \varphi_j(\mathbf{x}_k^{(j)})$.

It is standard to prove the optimal order approximation of the finite element solution.

THEOREM 3.1. *Let* $\{\varphi_i\}$ *be a set of nonoverlapping* C^1 *coordinate charts on* M, *defined in* (2.4). *There is a unique solution* u_h *to the finite element equations* (3.4). *It approximates the solution to* (2.1) *at the optimal order,*

$$\|u - u_h \circ \varphi^{-1}\|_{H^1(M)} \le Ch^k \|u\|_{H^k(M)},$$

where the solution $u \in C^\infty(M)$ *is smooth on the compact manifold* M, *and* $\varphi : \cup\Omega_i \to M$, *defined by* $\varphi|_{\Omega_i} = \varphi_i$.

Proof. Letting $v_h = u_h$ (3.4), we found the coerciveness of the bilinear form

$$a(u_h, u_h) = \|u_h \circ \varphi^{-1}\|_a^2 > 0,$$

where $\|\cdot\|_a$ denote the energy norm on Sobolev space $H^1(M)$ on the manifold M. By the Lax–Milgram theorem [6], (3.4) has a unique solution. By the orthogonal projection property,

$$\begin{aligned}\|u - u_h \circ \varphi^{-1}\|_{H^1(M)}^2 &= Ca(u \circ \varphi - u_h, u \circ \varphi - u_h)\\ &\le C\|u \circ \varphi - u_h\|_a \inf_{v \in V_h} \|u \circ \varphi - v\|_a\\ &\le C\|u - u_h \circ \varphi^{-1}\|_{H^1(M)} h^k \|u\|_{H^k(M)},\end{aligned}$$

where we apply (with a little adaptation) the Bramble–Hilbert lemma [6]. ∎

However, the bilinear forms in (3.4) cannot be evaluated exactly by numerical quadratures if $g_i^{\alpha\beta}$, $\sqrt{G^{(i)}}$, and $f(\varphi_i^{-1}(\mathbf{x}))$ are not polynomials. These are called variational crimes. The treatment is standard. That is, each chart Ω_i is covered by parametric elements of degree k such that the finite element referencing mappings (cf. [4]) vanish at the Lobatto boundary nodes (not unique in high space dimension). Then if the boundary of Ω_i is piecewise smooth, we have the following bound on the perturbation due to boundary approximation (cf. Theorem 10.2.36 in [4]):

$$\left|\Omega_i \setminus \cup_{T \in \mathcal{T}_{(i),h}} T\right| \le Ch^{k+1}, \tag{3.5}$$

where each T is an n-simplex with possibly one P_k face. Let us denote the parametric finite element space on the perturbed domains by $\tilde{V}_h^{(i)}$. The bilinear form approximation is also standard when choosing high enough order of quadratures (cf. Theorem

10.4.8 in [4]):

$$\sup_{\tilde{v}\in\tilde{V}_h^{(i)}\setminus\{0\}} \frac{|a_h(\tilde{u}_h,v)-a(u_h,\tilde{v})|}{\|\tilde{v}\|_{H^1(\Omega_i}} \le Ch^k\|u_h\|_{H^{k+1}(\Omega_i)}, \tag{3.6}$$

$$\sup_{\tilde{v}\in\tilde{V}_h^{(i)}\setminus\{0\}} \frac{|(f,v)_h-(f,\tilde{v})|}{\|\tilde{v}\|_{L^2(\Omega_i}} \le Ch^k\|f\|_{W^1_\infty(\Omega_i)}. \tag{3.7}$$

COROLLARY 3.2. *Suppose the domains Ω_i and bilinear forms are well approximated; i.e.,* (3.5)–(3.7) *hold. Then the perturbed finite element solution converges at the optimal order too:*

$$\|u-\tilde{u}_h\circ\varphi^{-1}\|_{H^1(\tilde{M})} \le Ch^k\|u\|_{H^k(M)},$$

where $\tilde{u}_h\in\tilde{V}_h=\{\tilde{v}|_{\gamma_{ij}}=\tilde{v}|_{\gamma_{ji}} \mid v\in\tilde{V}_h^{(i)}\}$ such that

$$a_h(\tilde{u}_h,\tilde{v})=(f,\tilde{v})_h \quad \forall\tilde{v}\in\tilde{V}_h. \qquad \square$$

Next, we introduce a finite element method for (2.1) with overlapping coordinate charts $\{\varphi_i\}$ from (2.6). However, we have a very strong assumption that the grids on Ω_i and Ω_j are mapped to the same grid on the overlapping portion $M_j\cap M_i$ on M in (3.1). This assumption is to simplify the implementation techniques. If the grids on overlapping regions are nonmatching, some nodal interpolation would be introduced to transfer functions from $V_h^{(i)}$ to $V_h^{(j)}$. As usual, we do not consider numerical integration error. Otherwise the grid size h in Theorems 3.1 and 3.3 has to be sufficiently small, depending on the smoothness of M and the smoothness of coordinates φ_i. The finite element problem for the overlapping variational problem (2.7) is as follows: find $u_h\in V_h$ such that

$$a_i(u_h,v_h)=(f,v_h) \quad \forall v_h\in V_h^{(i)}\cap H_0^1(\Omega_i),\ i=1,\dots,K, \tag{3.8}$$

where $a_i(\cdot,\cdot)$ is defined after (3.4).

THEOREM 3.3. *Let $\{\varphi_i\}$ be a set of general, overlapping coordinate charts on M, defined in* (2.6). *There is a unique solution u_h to the finite element equations* (3.8). *It approximates the solution to* (2.1) *at the optimal order,*

$$\|u-u_h\circ\varphi^{-1}\|_{H^1(M)} \le Ch^k\|u\|_{H^k(M)},$$

where the solution $u\in C^\infty(M)$ is smooth on the compact manifold M.

Proof. The uniqueness of the solution to (3.8) is proved exactly the same way as its continuous version (2.3), as we assume a grid matching (3.1) and no numerical quadrature error. By (3.8),

$$a(u\circ\varphi-u_h,v_h)=0 \quad \forall v_h\in V_h^{(i)}\cap H_0^1(\Omega_i).$$

Due to interior overlapping, for all nodal basis functions ϕ_l,

$$a(u\circ\varphi-u_h,\phi_l)=0 \quad \forall\phi_l\in V_h.$$

That is, the a-orthogonal projection property is kept in (3.8). Thus

$$\begin{aligned}\|u-u_h\circ\varphi^{-1}\|^2_{H^1(M)} &= Ca(u\circ\varphi-u_h,u\circ\varphi-u_h)\\ &\le C\|u\circ\varphi-u_h\|_a \inf_{v\in V_h}\|u\circ\varphi-v\|_a\\ &\le C\|u-u_h\circ\varphi^{-1}\|_{H^1(M)}h^k\|u\|_{H^k(M)}. \qquad \square\end{aligned}$$

4. Numerical experiments. We perform three numerical tests on a sphere S^3 in R^4 with nonoverlapping charts or overlapping charts. We then compare the traditional surface finite element method and the flat finite element method numerically by an S^2 problem.

4.1. A global S^3 problem (with C^1 charts). Let

$$M = S^3 = \left\{ (y_1, y_2, y_3, y_4) \in R^4 \;\middle|\; \sum y_i^2 = 1 \right\}.$$

For nonoverlapping charts (2.4), we cut S^3 along its equator $\{y_4 = 0\}$ (see Figure 3) to get the upper hemisphere M_1 and the lower hemisphere M_2. We use stereographic projection from the south pole $(0, 0, 0, -1)$ and north pole $(0, 0, 0, 1)$ to give M_1 and M_2 coordinate charts, respectively; see Figure 4, where S and N are the poles, P is on the sphere, and Q is on the R^3-hyperplane. We give the coordinates of Q to P, that is,

$$\varphi_i \; : P \mapsto Q, \quad \varphi_i \; : \Omega_i \to M_i. \tag{4.1}$$

Under these two coordinate charts, both Ω_i for M_1 and M_2 are the 3-dimensional unit ball:

$$B^3 = \Omega_1 = \Omega_2 = \{(x_1, x_2, x_3) \in R^3 \mid x_1^2 + x_2^2 + x_3^2 \le 1\}. \tag{4.2}$$

The grids on Ω_i are standard multigrids [35], displayed in Figure 5.

The Riemannian metric is

$$\frac{4}{(|\mathbf{x}|^2 + 1)^2}(dx_1 \otimes dx_1 + dx_2 \otimes dx_2 + dx_3 \otimes dx_3), \tag{4.3}$$

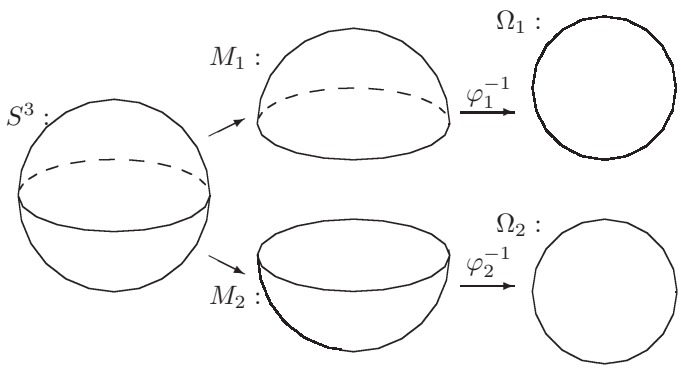

FIG. 3. *Two nonoverlapping C^1 charts for S^3; cf.* (2.4) *and* (4.1).

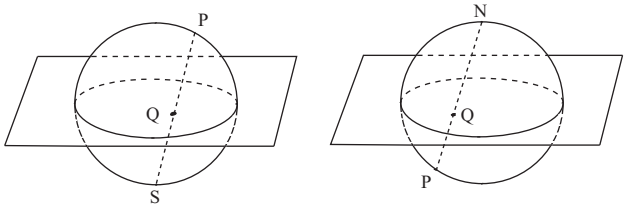

FIG. 4. *Projections defining charts φ_1 (left) and φ_2 (right); cf.* (4.1).

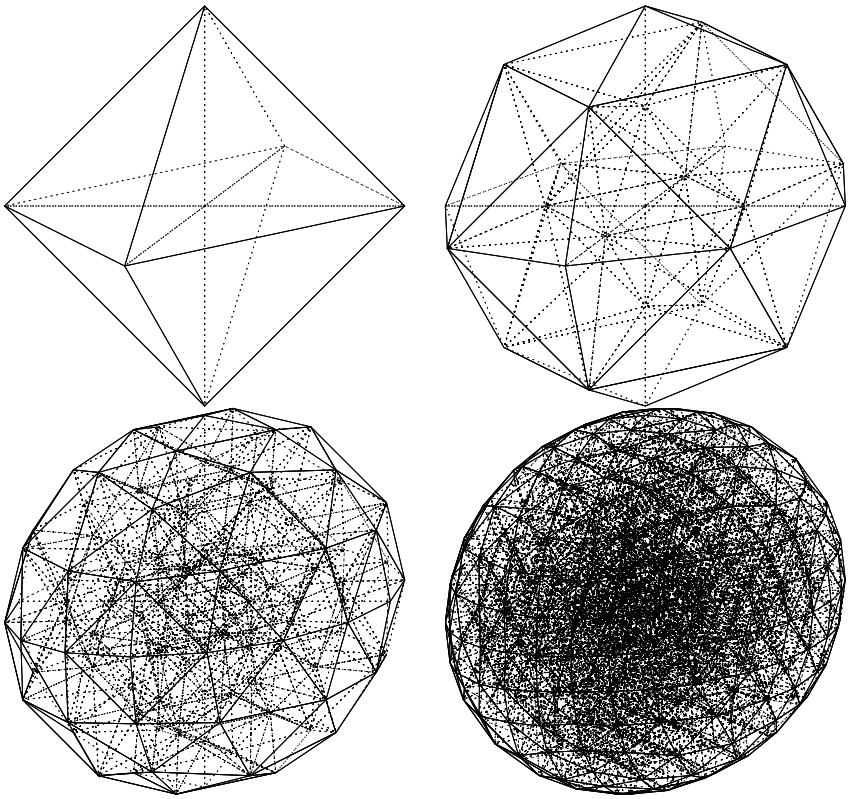

FIG. 5. *First 4 grids* $\mathcal{T}_{(i),h}$ *on* $\Omega_i = B_3$*; cf.* (4.2) *and Table* 1.

where $|\mathbf{x}|^2 = x_1^2 + x_2^2 + x_3^2$. The matrix $(g_{\alpha,\beta})_{3\times 3}$ is $\frac{4}{(|\mathbf{x}|^2+1)^2} I_{3\times 3}$. This computation can be found in many textbooks of Riemannian geometry, for example, p. 33 in [23]. Thus we have, in both M_1 and M_2,

$$\Delta_S u = \frac{(|\mathbf{x}|^2+1)^2}{4}\left(\sum_{i=1}^{3}\frac{\partial^2 u}{\partial x_i^2}\right) - \frac{|\mathbf{x}|^2+1}{2}\left(\sum_{i=1}^{3} x_i \frac{\partial u}{\partial x_i}\right),$$

$$\langle \nabla u, \nabla v\rangle = \frac{(|\mathbf{x}|^2+1)^2}{4}\left(\sum_{i=1}^{3}\frac{\partial u}{\partial x_i}\frac{\partial v}{\partial x_i}\right).$$

We solve the following equation on the sphere S^3,

$$-\Delta_S u + u = f, \tag{4.4}$$

where

$$f = 4y_4$$

and y_4 is the last coordinate of R^4. This equation has a unique analytic solution

$$u = y_4,$$

TABLE 1
The error (on M_1) and order for (4.5).

	$\|I_h u - u_h\|_{L^2}$	h^n	$\|I_h u - u_h\|_{l^\infty}$	h^n	$\|I_h u - u_h\|_{H^1}$	h^n	#CG
1	0.146367		0.400843		0.8016854972		2
2	0.092666	0.7	0.217679	0.9	0.4451659853	0.8	4
3	0.028304	1.7	0.075876	1.5	0.1492563307	1.6	14
4	0.007812	1.9	0.023080	1.7	0.0483691271	1.6	36
5	0.002050	1.9	0.007179	1.7	0.0146292349	1.7	74
6	0.000522	2.0	0.002143	1.7	0.0042019146	1.8	150

which is a height function of the sphere S^3. On local coordinate charts, we have

$$u = \begin{cases} \dfrac{-x_1^2 - x_2^2 - x_3^2 + 1}{x_1^2 + x_2^2 + x_3^2 + 1} & \text{in } \Omega_1, \\ \dfrac{x_1^2 + x_2^2 + x_3^2 - 1}{x_1^2 + x_2^2 + x_3^2 + 1} & \text{in } \Omega_2. \end{cases} \tag{4.5}$$

We compute the problem with conforming P_1 finite element, i.e., $k = 1$ in (3.2). First, we solve the global finite element directly by the conjugate gradient method. Due to symmetry, only the top half problem is solved. That is, we solve the following problem on half of Ω_1:

$$a_{1/2}(u_h, v_h) = (f, v_h)_{1/2}, \quad v_h \in V_h^{(1)} \cap H_0^1(B_3),$$

where $V_h^{(1)}$ is defined in (3.2), B_3 is defined in (4.2), and

$$a_{1/2}(u_h, v_h) = \int_{B^3} \left(\frac{2}{|\mathbf{x}|^2 + 1} \sum_{j=1}^{3} \frac{\partial u_h}{\partial x_j} \frac{\partial v_h}{\partial x_j} + \frac{8 u_h v_h}{(|\mathbf{x}|^2 + 1)^3} \right) dx_1 dx_2 dx_3,$$

$$(f, v_h)_{1/2} = \int_{B^3} \frac{32(1 - |\mathbf{x}|^2) v_h}{(|\mathbf{x}|^2 + 1)^4} dx_1 dx_2 dx_3.$$

The number of conjugate gradient iterations are listed in the last column of Table 1. The convergence order is optimal, as predicted by Theorem 3.1. We note that we have a superconvergence in the H^1 norm (see the seventh column of Table 1). This is consistent with the work of [33], where a surface triangulation is applied to S^2. But the superconvergence is not proved in our paper here.

4.2. A nonoverlapping S^3 problem (with C^1 charts). We solve (4.4) again, where the exact solution is still (4.5). We experiment using the nonoverlapping domain decomposition method. We solve the finite element equations by the Robin–Robin nonoverlapping domain decomposition method [24, 9, 27, 28]. The coordinate charts for M_1 and M_2 are defined in (4.1) and (4.2),

$$\varphi_i : \Omega_i \to M_i, \quad i = 1, 2.$$

However, we also have boundary integrals this time. The coordinate charts for ∂M_1 and ∂M_2 are the unit sphere too, but in R^3, i.e.,

$$S^2 = \partial M_1 = \partial M_2 = \{(x_1, x_2, x_3) \in R^3 \mid x_1^2 + x_2^2 + x_3^2 = 1\}.$$

The Riemannian metric matrix on the boundary integral is just I, the identity matrix. We get the iteration scheme as follows:

$$a_i(u_{h,n}^{(i)}, v_h^{(i)}) + \lambda \int_{\partial M_i} \pi_i u_{h,n}^{(i)} \cdot \pi_i v_h^{(i)} = (f, v_h^{(i)}) + \int_{\partial M_i} r_i^n \cdot \pi_i v_h^{(i)}, \tag{4.6}$$

$$r_i^{n+1} = 2\lambda \cdot \pi_j u_{h,n}^{(j)} - r_j^n,$$

where λ is a Robin–Robin domain decomposition parameter (we choose 1 for it in the computation), $i, j \in \{1, 2\}$, $u_{h,n}^{(i)}$ is the nth iteration solution on M_i, the operator π_i is the trace operator on ∂M_i, and

$$a_i(u_{h,n}^{(i)}, v_h^{(i)}) = \int_{M_i} \left(\frac{2}{1+|\mathbf{x}|^2} \sum_{j=1}^{3} \frac{\partial u_{h,n}^{(i)}}{\partial x_j} \frac{\partial v_h^{(i)}}{\partial x_j} + \frac{8}{(|\mathbf{x}|^2+1)^3} u_{h,n}^{(i)} v_h^{(i)} \right) dx_1 dx_2 dx_3, \tag{4.7}$$

$$(f, v_i) = \int_{M_i} \frac{32(1-|\mathbf{x}|^2) v_h^{(i)}}{(|\mathbf{x}|^2+1)^4} dx_1 dx_2 dx_3. \tag{4.8}$$

The boundary integral on ∂M_i in (4.6) is computed via coordinate charts Ω_i and Ω_j. (For more details about the above procedure, see [27].) The computational results are listed in Table 2. The number of domain decomposition iterations is listed in the last column. Here the iteration stops until the difference between the last two iterates is less than 10^{-5}.

TABLE 2
The error and order by nonoverlapping domain decomposition, (4.5).

	$\|I_h u - u_h\|_{L^2}$	h^n	$\|I_h u - u_h\|_{l^\infty}$	h^n	$\|I_h u - u_h\|_{H^1}$	h^n	#dd
1	0.204792		0.560723		1.1212842055		25
2	0.149337	0.5	0.363531	0.6	0.6285882667	0.8	25
3	0.057322	1.4	0.146772	1.3	0.2329487210	1.4	27
4	0.016304	1.8	0.047581	1.6	0.0701729023	1.7	27
5	0.004372	1.9	0.014098	1.8	0.0192478986	1.9	28
6	0.001178	1.9	0.004029	1.8	0.0050866812	1.9	28

4.3. An overlapping S^3 problem. As the third numerical test on S^3, solving (4.4), we choose an overlapping set of charts for the manifold S^3. Since it would be difficult to make the piecewise charts C^1 across the boundary, it is more practical to consider overlapping charts where the C^1 continuity requirement is relaxed. That is, we use the second method, the overlapping domain decomposition method. In our test, we solve problem (4.4) again with the solution (4.5). This time, φ_1 and φ_2 are defined the same way as (4.1), except they are extended further to the other half of the sphere, as shown in Figure 6. We choose Ω_i to be a 3-dimensional sphere of radius 2 (not radius 1 as above):

$$\Omega_1 = \Omega_2 = \left\{ (x_1, x_2, x_3) \in R^3 \mid x_1^2 + x_2^2 + x_3^2 \le 2^2 \right\}. \tag{4.9}$$

Then

$$M_1 = \left\{ (y_1, y_2, y_3, y_4) \in S^3 \mid y_4 \ge -\frac{3}{5} \right\},$$

$$M_2 = \left\{ (y_1, y_2, y_3, y_4) \in S^3 \mid y_4 \le \frac{3}{5} \right\}.$$

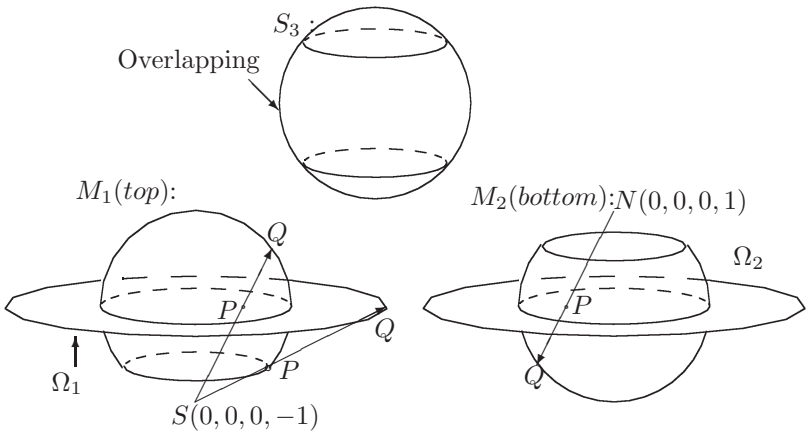

FIG. 6. *Overlapping M_1 and M_2 ($y_4 = \mp 3/5$); cf.* (2.6) *and* (4.9).

TABLE 3
The error (bigger M_1) and order by overlapping domain decomposition, (4.10).

	$\|I_h u - u_h\|_{L^2}$	h^n	$\|I_h u - u_h\|_{l^\infty}$	h^n	$\|I_h u - u_h\|_{H^1}$	h^n	#dd
3	0.493551		0.341005		0.9633354454		6
4	0.138991	1.8	0.127412	1.4	0.2774985855	1.8	6
5	0.038944	1.8	0.040861	1.6	0.0765976372	1.9	6
6	0.010936	1.8	0.012113	1.8	0.0207526761	1.9	6

We perform an overlapping domain decomposition method to solve (3.4). That is, given $u_{h,0}^{(2)} = 0$, we shall find $u_{h,n}^{(1)}$ and $u_{h,n}^{(2)}$, $n = 1, 2, \ldots$, by

$$\begin{cases} a_1(u_{h,n}^{(1)}, v_h^{(1)}) = (f, v_h^{(1)}) & \forall v_h^{(1)} \in V^{(1)}, \\ u_{h,n}^{(1)}|_{\partial M_1} = u_{h,n-1}^{(2)}, \end{cases} \tag{4.10}$$

$$\begin{cases} a_2(u_{h,n}^{(2)}, v_h^{(2)}) = (f, v_h^{(2)}) & \forall v_h^{(2)} \in V^{(2)}, \\ u_{h,n}^{(2)}|_{\partial M_2} = u_{h,n-1}^{(1)}. \end{cases} \tag{4.11}$$

Here $a_i(\cdot,\cdot)$ and $(f,\cdot)$ are defined in (4.7) and (4.8), respectively. Note that, due to overlapping, the boundary of M_1 is in the interior of M_2, as shown in Figure 6. Due to a big overlap, the domain decomposition converges very fast. Only 6 iterations are needed to reach a 10^{-5} difference. The numerical results are listed in Table 3. We note that, because the computation domain is twice as big as in the last computation, a radius 2 ball in 3 dimensions, the errors in Table 3 are bigger than those listed in Tables 1 and 2. We note that the computation starts from grid 3 in Table 3. This is because we need the boundary data of $u_{h,n}^{(1)}$ from the iterate $u_{h,n-1}^{(2)}$ at some interior grid points, that is,

$$u_{h,n}^{(1)} \circ \varphi_1^{-1}|_{x_1^2+x_2^2+x_2^2=2^2} = u_{h,n-1}^{(2)} \circ \varphi_2^{-1}|_{x_1^2+x_2^2+x_2^2=\left(\frac{1}{2}\right)^2}.$$

4.4. A comparison of the surface/flat finite element methods. We choose a numerical problem on the 2-sphere $S^2 = \{(y_1, y_2, y_3) \in R^3 \mid \sum y_i^2 = 1\}$:

$$-\Delta_S u + 2u = f \qquad \text{on } S^2, \tag{4.12}$$

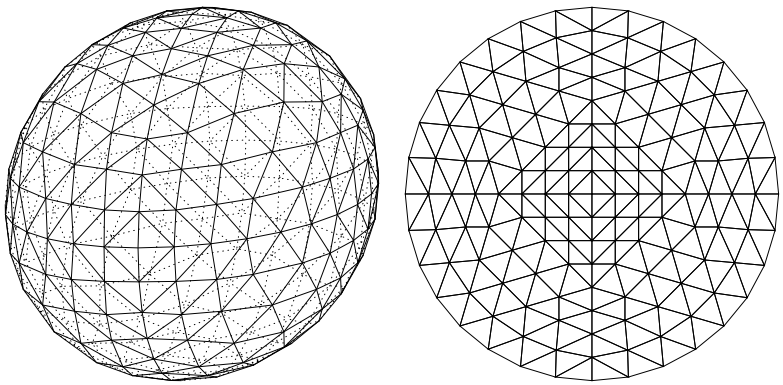

FIG. 7. *Level 4 surface grid on S^2, and flat grid on B^2.*

TABLE 4
The error of surface finite element method for (4.1) *and* (4.14).

	$\|I_h u - u_h\|_{L^2}$	h^n	$\|I_h u - u_h\|_{l^\infty}$	h^n	$\|I_h u - u_h\|_{H^1}$	h^n	#cg
1	0.358190	0.0	0.333333	0.0	0.71637	0.0	2
2	0.187844	0.9	0.148472	1.2	0.32505	1.1	3
3	0.059300	1.7	0.051167	1.5	0.10593	1.6	7
4	0.015848	1.9	0.015892	1.7	0.03024	1.8	21
5	0.004037	2.0	0.004709	1.8	0.00824	1.9	45
6	0.001015	2.0	0.001357	1.8	0.00220	1.9	93
7	0.000254	2.0	0.000384	1.8	0.00058	1.9	188

where

$$f = 4y_3. \tag{4.13}$$

The exact solution of (4.12) is

$$u = y_3. \tag{4.14}$$

Using surface grids shown in the left graph of Figure 7, we derive surface finite element equations, which are solved by the conjugate gradient iteration. The error between the interpolation and the finite element solution is listed in Table 4, in the L^2 norm, l^∞ norm, and H^1 seminorm. Here we get a superconvergence for the error in the H^1 seminorm, as proved by [33], i.e., an order two convergence instead of order one, the optimal order.

Now, we use the local-chart finite element method to solve problem (4.12). This time, we have flat grids, shown in the right graph of Figure 7, the 4th level grid, on

$$\Omega_1 = \Omega_2 = B^2 = \{(x_1, x_2) \in R^2 \mid x_1^2 + x_2^2 \le 1\}. \tag{4.15}$$

Similar to the first example in subsection 4.1, we have only two charts. Then using symmetry, we solve only half of the problem (top half of (4.1)), where on the chart B^2 the solution (4.14) is

$$u(x_1, x_2) = \frac{1 - |\mathbf{x}|^2}{1 + |\mathbf{x}|^2}, \tag{4.16}$$

and the right-hand side function of (4.12) is

$$f(x_1, x_2) = \frac{4(1-|\mathbf{x}|^2)}{1+|\mathbf{x}|^2}, \tag{4.17}$$

where $|\mathbf{x}|^2 = x_1^2 + x_2^2$. The variational form for (4.12) is

$$a_i(u_h^{(i)}, v_h^{(i)}) = (f, v_h^{(i)}) \quad \forall v_h^{(i)} \in V^{(i)}, \tag{4.18}$$

where $V^{(i)}$ is defined in (3.2), a linear finite element space on B^2. In (4.18),

$$a_i(u_h^{(i)}, v_h^{(i)}) = \int_{B^2} \left(\sum_{j=1}^{2} \frac{\partial u_h^{(i)}}{\partial x_j} \frac{\partial v_h^{(i)}}{\partial x_j} + \frac{8 u_h^{(i)} v_h^{(i)}}{(1+|\mathbf{x}|^2)^2} \right) dx_1 dx_2, \tag{4.19}$$

$$(f, v_h^{(i)}) = \int_{B^2} \frac{16(1-|\mathbf{x}|^2) v_h^{(i)}}{(1+|\mathbf{x}|^2)^3} dx_1 dx_2. \tag{4.20}$$

TABLE 5
The error of flat finite element method for (4.1) *and* (4.16).

	$\|I_h u - u_h\|_{L^2}$	h^n	$\|I_h u - u_h\|_{l^\infty}$	h^n	$\|I_h u - u_h\|_{H^1}$	h^n	#cg
1	0.037771	0.0	0.065421	0.0	0.130841	0.0	2
2	0.075449	0.0	0.183233	0.0	0.309065	0.0	3
3	0.021610	1.8	0.070465	1.4	0.114926	1.4	7
4	0.006126	1.8	0.023310	1.6	0.035071	1.7	21
5	0.001598	1.9	0.007093	1.7	0.009718	1.9	52
6	0.000405	2.0	0.002070	1.8	0.002608	1.9	108
7	0.000102	2.0	0.000590	1.8	0.000691	1.9	218
8	0.000025	2.0	0.000166	1.8	0.000182	1.9	439
9	0.000006	2.0	0.000046	1.9	0.000048	1.9	879

The error between the interpolation and the finite element solution is listed in Table 5, in the L^2 norm, l^∞ norm, and H^1 seminorm, on B^2. Here we also have a superconvergence for the error in the H^1 seminorm. But it is not proved in this paper. Comparing Tables 4 and 5, the two methods are about the same. But the implementation of the flat finite element method is much simpler than that of the surface finite element method. Also, in our implementation, the flat finite element method takes only 1.031 seconds CPU time (on a Toshiba laptop, Satellite A135-S4656 of Intel 1.6GHz Celeron M Processor 520 and 512MB DDR2 RAM), but 26.942 seconds CPU time for the surface finite element method, both up to the level 7 computation. We note that about 1/3 of the computation time in the surface finite element method is used for surface grid generation. By our estimate, if all is optimized, the surface finite element method may take about twice as much time as that of the flat finite element method, not 26 times.

Acknowledgment. We thank the anonymous referees for many constructive comments and suggestions which led to an improved presentation of this paper.

REFERENCES

[1] D. N. ARNOLD, A. MUKHERJEE, AND L. POULY, *Adaptive finite elements and colliding black holes*, in Numerical Analysis 1997 (Dundee), Pitman Res. Notes Math. Ser. 380, Longman, Harlow, 1998, pp. 1–15.

[2] E. Bansch, P. Morin, and R. H. Nochetto, *A finite element method for surface diffusion: The parametric case*, J. Comput. Phys., 203 (2005), pp. 321–343.
[3] S. Bartels, *Stability and convergence of finite element approximation schemes for harmonic maps*, Math. Comp., 79 (2010), pp. 1263–1301.
[4] S. C. Brenner and L. R. Scott, *The Mathematical Theory of Finite Element Methods*, 3rd ed., Springer, New York, 2008.
[5] T. F. Chan and T. P. Mathew, *Domain decomposition algorithms*, in Acta Numerica 1994, Cambridge University Press, Cambridge, UK, 1994, pp. 61–143.
[6] P. G. Ciarlet, *The Finite Element Method for Elliptic Problems*, North-Holland, Amsterdam, 1978.
[7] A. Demlow, *Higher-order finite element methods and pointwise error estimates for elliptic problems on surfaces*, SIAM J. Numer. Anal., 47 (2009), pp. 805–827.
[8] A. Demlow and G. Dziuk, *An adaptive finite element method for the Laplace–Beltrami operator on implicitly defined surfaces*, SIAM J. Numer. Anal., 45 (2007), pp. 421–442.
[9] Q. Deng, *An analysis for a nonoverlapping domain decomposition iterative procedure*, SIAM J. Sci. Comput., 18 (1997), pp. 1517–1525.
[10] Q. Deng, *A nonoverlapping domain decomposition method for nonconforming finite element problems*, Comm. Pure Appl. Anal., 2 (2003), pp. 295–306.
[11] G. de Rham, *Variétés Différentiables*, Hermann, Paris, 1973.
[12] T. A. Driscoll, *A nonoverlapping domain decomposition method for Symm's equation for conformal mapping*, SIAM J. Numer. Anal., 36 (1999), pp. 922–934.
[13] Q. Du and L. Ju, *Finite volume methods on spheres and spherical centroidal Voronoi meshes*, SIAM J. Numer. Anal., 43 (2005), pp. 1673–1692.
[14] G. Dziuk, *Finite elements for the Beltrami operator on arbitrary surfaces*, in Partial Differential Equations and Calculus of Variations, Lecture Notes in Math. 1357, Springer, Berlin, 1988, pp. 142–155.
[15] G. Dziuk and C. M. Elliott, *Finite elements on evolving surfaces*, IMA J. Num. Anal., 27 (2007), pp. 262–292.
[16] M. J. Gander and G. H. Golub, *A nonoverlapping optimized Schwarz method which converges with an arbitrarily weak dependence on h*, in Proceedings of the Fourteenth International Conference on Domain Decomposition Methods, 2002.
[17] M. J. Gander, L. Halpern, and F. Nataf, *Optimized Schwarz methods*, in Proceedings of the Twelfth International Conference on Domain Decomposition Methods, Chiba, Japan, 2001, pp. 15–28.
[18] C. F. Gauss, *Werke: Herausgegeben von der Koniglichen Gesellschaft der Wissenschaften zu Gottingen*, 1838, Georg Olms, Verlag, New York, 1981.
[19] E. Hopf, *Elementare Bemarkungen über die Lösungen partieller Differentialgleichungen zweiter Ordnung vom elliptischen Typus. (Elementary remarks concerning second order elliptic partial differential equations)*, Sitzungsber. d. Preuss. Akad. d. Wiss., 19 (1927), pp. 147–152.
[20] L. V. Hörmander, *Linear Partial Differential Operators*, Grundlehren Math. Wiss. 116, Springer-Verlag, Berlin, 1963.
[21] J. Jost, *Riemannian Geometry and Geometric Analysis*, 4th ed., Springer, Berlin, 2005.
[22] O. Korobkin, B. Aksoylu, M. Holst, E. Pazos, and M. Tiglio, *Solving the Einstein constraint equations on multi-block triangulations using finite element methods*, Classical Quantum Gravity, 26 (2009), 145007.
[23] J. M. Lee, *Riemannian Manifolds: An Introduction to Curvature*, Grad. Texts in Math. 176, Springer-Verlag, New York, 1997.
[24] P. L. Lions, *On the Schwarz alternating method* III: *A variant for nonoverlapping subdomains*, in Proceedings of the Third International Symposium on Domain Decomposition Methods for Partial Differential Equations, 1990.
[25] J. Maes, A. Kunoth, and A. Bultheel, *BPX-type preconditioners for second and fourth order elliptic problems on the sphere*, SIAM J. Numer. Anal., 45 (2007), pp. 206–222.
[26] M. A. Olshanskii and A. Reusken, *A finite element method for surface PDEs: Matrix properties*, Numer. Math., 114 (2010), pp. 491–520.
[27] L. Qin and X. Xu, *On a parallel Robin-type nonoverlapping domain decomposition method*, SIAM J. Numer. Anal., 44 (2006), pp. 2539–2558.
[28] L. Qin and X. Xu, *Optimized Schwarz methods with Robin transmission conditions for parabolic problems*, SIAM J. Sci. Comput., 31 (2008), pp. 608–623.
[29] J.-F. Remacle, C. Geuzaine, G. Compre, and E. Marchandise, *High quality surface remeshing using harmonic maps*, Internat. J. Numer. Methods Engrg., 83 (2010), pp. 403–425.
[30] R. Schoen and S. T. Yau, *On univalent harmonic maps between surfaces*, Invent. Math., 44 (1978), pp. 265–278.

[31] R. Schoen and S. T. Yau, *Lectures on Differential Geometry*, International Press, Cambridge, MA, 1994.
[32] H. A. Schwarz, *Gesammelte Mathematische Abhandlungen*, Vol. 2, Springer, Berlin, 1890, pp. 133–143; first published in Vierteljahrsschrift der Naturforschenden Gesellschaft in Zürich, 15 (1870), pp. 272–286.
[33] H. Wei, L. Chen, and Y. Huang, *Superconvergence and gradient recovery of linear finite elements for the Laplace–Beltrami operator on general surfaces*, SIAM J. Numer. Anal., 48 (2010), pp. 1920–1943.
[34] J.-J. Xu and H.-K. Zhao, *An Eulerian formulation for solving partial differential equations along a moving interface*, J. Sci. Comput., 19 (2003), pp. 573–594.
[35] S. Zhang, *Successive subdivisions of tetrahedra and multigrid methods on tetrahedral meshes*, Houston J. Math., 21 (1995), pp. 541–556.
[36] G. Zumbusch, *Finite element, discontinuous Galerkin, and finite difference evolution schemes in spacetime*, Classical Quantum Gravity, 26 (2009), 175011.